Vector gap solitons of spin-orbit-coupled Bose-Einstein condensate in honeycomb optical lattices

Hongjuan Meng, Jing Wang, Xiaobei Fan, Qingqing Wang, Kaihua Shao, Yuexin Zhao, Wenyuan Wang,* and Yuren Shi†
College of Physics and Electronic Engineering, Northwest Normal University, Lanzhou 730070, China
and Key Laboratory of Atomic and Molecular Physics and Functional Materials of Gansu Province, Northwest Normal University, Lanzhou 730070, China

(Received 20 August 2023; accepted 6 September 2023; published 28 September 2023)

The combination of the two hot topics of spin-orbit coupling and honeycomb lattices leads to the appearance of fascinating issues. In this paper, we investigate the existence and stability of vector gap solitons of spin-orbit-coupled Bose-Einstein condensates loaded in honeycomb optical lattices. The existence and stability of vector gap solitons are highly sensitive to the properties of interspin and intraspin atomic interaction. We numerically obtain the parametric dependence of the existence of vector gap solitons both in the semi-infinite gap and in the first gap. Since only dynamically stable localized modes in nonlinear systems are likely to be generated and observed in experiments, we examine the stability of the vector gap solitons by using the direct evolution dynamics, and obtain the phase diagram of stable and unstable vector gap solitons on the parameter plane of interspin and intraspin atomic interactions.

DOI: 10.1103/PhysRevE.108.034215

I. INTRODUCTION

Spin-orbit coupling (SOC) has attracted much attention in condensed matter studies for its essential role in many exotic phenomena, such as the realization of topological insulators [1–3], topological superconductors [2,4], spin Hall effects [5–7], Floquet topological phases [8,9], and so on. In ultracold atomic gases, SOC has been realized both in fermionic [10,11] and in bosonic [12,13] systems by Raman coupling. Since ultracold atoms provide a clean and ideal platform, the achievement of SOC has opened up a progressively growing interest in the physics of mixtures of spinor Bose-Einstein condensates (BECs) in studies of matter waves. Respectively, such objects as Skyrmions [14–16] and solitons [17–27] have been reported for spin-orbit (SO)-coupled BECs.

BECs loaded in periodic optical lattices were widely recognized as a particularly efficient manipulation of BECs [28], which can share many features with waves in nonlinear systems. In particular, the interplay of the intrinsic nonlinearity of BECs with the periodicity of optical lattices suggests possibilities for the creation of gap solitons, i.e., the existence of a novel kind of localized modes that reside in the linear energy gaps between the Bloch bands [29,30]. The creation of gap solitons has been predicted theoretically [31–35] and first experimentally observed in fiber Bragg gratings [36]. Gap solitons of BEC in optical lattices have been an active topic [28,37–39] and have been observed experimentally [40,41].

The SO-coupled spinor BEC in optical lattices offers new possibilities for creating gap solitons. In the aspect of gap solitons in spinor SO-coupled BECs, several studies have been devoted, such as bright profiles with repulsive atomic interaction [17], symmetries and stability in a periodic Zeeman field [42,43], existence and stability of multipole and half-vortex gap solitons in a lattice created by the Zeeman field [44], spin-dependent parity symmetry [45], existence and stability analysis in one-dimensional Zeeman lattices with attractive nonlinearity [46], quasi-one-dimensional existence and dynamics with SOC and time-varying Raman frequency [47], one- and two-dimensional existence and dynamics in free space with Zeeman splitting SOC [48,49], dipole gap solitons in microwave-mediated interaction induced trapping potentials [50], and two-dimensional gap solitons belonging to the semi-infinite gap created by periodically modulated SOC [51], to name only a few.

The underlying spatially periodic structures play a key role in producing spectral band gaps, in which gap solitons can be created. It was shown that the band structures of a SO-coupled quantum gas can be induced by an external periodic field, which leads to the appearance of new gaps [52,53]. Apart from the simple representative cubic optical lattice, past experiments with ultracold atoms have utilized exotic lattices such as triangular [54], honeycomb [55], and Kagome lattices [56]. Among them, honeycomb optical lattices can lead to significantly different results due to underlying symmetries. It is noteworthy that gap solitons in honeycomb optical lattices have been studied both theoretically and experimentally [57], such as in honeycomb photonic lattices [58,59] and dynamical lattices [60]. In previous studies by some of us [61,62], for the single-component BEC, gap solitons in honeycomb optical lattices have been investigated. However, as far as we know, for the SO-coupled BECs loaded in honeycomb optical lattices, there has been little work on the formation and dynamical properties of vector gap solitons. It is well known that the SOC provides a new degree of freedom to regulate striking interaction features of the localized structures and dynamics.

To fill the gap, in this paper, we investigate the formation and dynamical stability of vector gap solitons of SO-coupled

*wywang@nwnu.edu.cn
†shiyr@nwnu.edu.cn

two internal states of BECs loaded in honeycomb optical lattices. It is found that the two-dimensional honeycomb optical lattices admit vector gap solitons for SO-coupled BECs. The existence of vector gap solitons is dependent on the properties of atomic interactions. Interestingly, the two components of vector gap solitons always show phase separation regardless of whether interspin or intraspin atomic interactions are dominant. We numerically obtain the existence of vector gap solitons in the parameter plane of interspin and intraspin atomic interactions both in the semifinite gap and in the first gap. Based on the direct evolution of the coupled Gross-Pitaevskii equations, we examine the dynamic stability of vector gap solitons in the different regimes for both the semifinite gap and first gap, respectively. The phase diagram accurately reflects that the combined effects of interspin and intraspin atomic interaction on dynamic stabilities of vector gap solitons are obtained. Our results are of significance in the field of matter-wave studies. They also have potential applications in the investigation of localized structures in nonlinear optics.

The paper is organized as follows. In Sec. II, we formulate the theoretical model for SO-coupled BEC in honeycomb optical lattices. In Sec. III, the band-gap structures induced by the SOC and the existence of vector gap soliton are presented. In Sec. IV, we propose the nonlinear dynamics of vector gap solitons. Finally, the main results of the present paper are summarized in Sec. V.

II. THE MODEL

We consider a mixture of BECs composed of the two internal states of ^{87}Rb [63], and label them pseudospin up and pseudospin down, namely, $|\uparrow\rangle \equiv |F=1, m_F=0\rangle$ and $|\downarrow\rangle \equiv |F=1, m_F=-1\rangle$. The BECs with Rashba SOC are loaded in a honeycomb optical lattice. In real experiments, the system contains about 1.8×10^5 atoms [63]. Within the framework of zero temperature mean-field theory, where the quantum and thermal fluctuations are negligible, the dynamics of these SO-coupled BECs can be well approximated by the following coupled Gross-Pitaevskii equations:

$$\begin{aligned} i\hbar\frac{\partial}{\partial t}\Psi_\uparrow(\mathbf{r},t) &= \Big[-\frac{\hbar^2}{2m}\nabla^2 + V(\mathbf{r}) + g_{\uparrow\uparrow}|\Psi_\uparrow(\mathbf{r},t)|^2 \\ &\quad + g_{\uparrow\downarrow}|\Psi_\downarrow(\mathbf{r},t)|^2\Big]\Psi_\uparrow(\mathbf{r},t) + i\kappa\partial_-\Psi_\downarrow(\mathbf{r},t), \\ i\hbar\frac{\partial}{\partial t}\Psi_\downarrow(\mathbf{r},t) &= \Big[-\frac{\hbar^2}{2m}\nabla^2 + V(\mathbf{r}) + g_{\downarrow\uparrow}|\Psi_\uparrow(\mathbf{r},t)|^2 \\ &\quad + g_{\downarrow\downarrow}|\Psi_\downarrow(\mathbf{r},t)|^2\Big]\Psi_\downarrow(\mathbf{r},t) + i\kappa\partial_+\Psi_\uparrow(\mathbf{r},t). \end{aligned} \tag{1}$$

Here the condensate wave functions are normalized as $N_\sigma = \int|\Psi_\sigma(\mathbf{r},t)|^2 d\mathbf{r}$ with $\Psi_\sigma(\mathbf{r},t)(\sigma=\downarrow,\uparrow)$ being the wave function of the spin-σ component, while the total number of atoms, i.e., the sum of numbers $N_\uparrow$ and $N_\downarrow$ of atoms of the spin σ, is $N = N_\uparrow + N_\downarrow$. m is the atom mass and $g_{\sigma\sigma'} = \frac{4\pi\hbar^2 a_{\sigma\sigma'}}{m}$ with $a_{\sigma\sigma'}$ being the s-wave scattering lengths between the species where spin σ and spin σ' denote the intra- and interspin interaction $g_{\sigma\sigma}$ and $g_{\uparrow\downarrow}$, respectively. To highlight the effects of intercomponent contact interaction, we further fix the intracomponent interactions as $g_{\uparrow\uparrow} = g_{\downarrow\downarrow}$, which is most closely relevant to the ^{87}Rb system [64]. κ represents the strength of SOC, and $\partial_\pm = \partial/\partial x \pm i\partial/\partial y$.

In what follows, we assume that the condensed atoms are trapped in a very thin honeycomb potential, i.e., the trapping potential in the x-y plane is much weaker than that in the z direction. In this case, the external trapping potential is given by the two-dimensional potential $V(\mathbf{r})$ that constructs the honeycomb optical lattice, which can be realized experimentally by superposing three coplanar traveling laser beams [65,66]. The three coplanar traveling laser beams have the same angular frequency $\omega_L = ck_0$ with k_0 the wave vector of the radiation. Then, the lattice potential can be denoted by [67]

$$V(\mathbf{r}) = V_0\left|e^{ik_0\mathbf{b}_1\cdot\mathbf{r}} + \eta_1 e^{ik_0\mathbf{b}_2\cdot\mathbf{r}} + \eta_2 e^{ik_0\mathbf{b}_3\cdot\mathbf{r}}\right|^2, \tag{2}$$

where $V_0 > 0$ is optical depth, $\mathbf{b}_1 = (0,1)$, $\mathbf{b}_2 = (-\frac{\sqrt{3}}{2}, -\frac{1}{2})$, $\mathbf{b}_3 = (\frac{\sqrt{3}}{2}, -\frac{1}{2})$, and η_1 and η_2 are relative intensities of the plane wave. Following Ref. [67], we only consider the same intensity case where $\eta_1 = \eta_2 = \eta > 0$. In order to form a honeycomb lattice, the condition $\eta > \frac{1}{2}$ should be satisfied. When the polarizations of all three waves are parallel, i.e., $\eta = 1$, the optical lattice has a perfect hexagonal structure similar to graphene. In this paper, we consider a standard honeycomb optical lattice and take $\eta = 1$.

After integrating out the z coordinates, we obtain the following quasi-two-dimensional dimensionless equations for the x-y plane of the wave functions:

$$\begin{aligned} i\frac{\partial}{\partial t}\Psi_\uparrow(\mathbf{r},t) &= [-\nabla^2 + V(\mathbf{r}) + g_{\uparrow\uparrow}|\Psi_\uparrow(\mathbf{r},t)|^2 \\ &\quad + g_{\uparrow\downarrow}|\Psi_\downarrow(\mathbf{r},t)|^2]\Psi_\uparrow(\mathbf{r},t) + i\kappa\partial_-\Psi_\downarrow(\mathbf{r},t), \\ i\frac{\partial}{\partial t}\Psi_\downarrow(\mathbf{r},t) &= [-\nabla^2 + V(\mathbf{r}) + g_{\downarrow\uparrow}|\Psi_\uparrow(\mathbf{r},t)|^2 \\ &\quad + g_{\downarrow\downarrow}|\Psi_\downarrow(\mathbf{r},t)|^2]\Psi_\downarrow(\mathbf{r},t) + i\kappa\partial_+\Psi_\uparrow(\mathbf{r},t). \end{aligned} \tag{3}$$

In the dimensionless units adopted above, the energy scale is in units of $4\hbar^2k_0^2/m$, the length scale is in units of $1/2\sqrt{2}k_0$, the time scale is in units of $m/4\hbar k_0^2$, and the wave function $\Psi_{1,2}$ is in units of $\sqrt{n_0}$ with n_0 the averaged BEC density, respectively.

III. BAND-GAP STRUCTURE AND THE EXISTENCE OF VECTOR GAP SOLITONS

This section is devoted to presenting the numerical results of the vector gap solitons of SO-coupled BEC loaded in honeycomb optical lattices, with an emphasis on how the intra- and interspin interaction would affect the formation of localized modes. It starts by providing the band-gap structure of the underlying linear periodic physical model. Then, the structures of vector gap solitons both in the semifinite gap and in the first band gap are produced numerically.

A. Band-gap structure

In order to investigate the formation of vector gap solitons, we first need to know the relevant band-gap structure of SO-coupled BEC in honeycomb optical lattices. This is achieved by taking the spinor wave function of Eq. (3) with the following form:

$$\Psi_{\uparrow,\downarrow}(\mathbf{r},t)=\psi_{\uparrow,\downarrow}(\mathbf{r})e^{-i\mu t}, \tag{4}$$

where μ is a real chemical potential. Substituting Eq. (4) into Eq. (3) leads to a set of stationary equations for the wave functions $\psi_\sigma(\mathbf{r})$:

$$\begin{aligned}\mu\psi_\uparrow(\mathbf{r}) =& -\left(\frac{\partial^2}{\partial x^2}+\frac{\partial^2}{\partial y^2}\right)\psi_\uparrow(\mathbf{r})+V(\mathbf{r})\psi_\uparrow(\mathbf{r})\\ &+g_{\uparrow\uparrow}|\psi_\uparrow(\mathbf{r})|^2\psi_\uparrow(\mathbf{r})+g_{\uparrow\downarrow}|\psi_\downarrow(\mathbf{r})|^2\psi_\uparrow(\mathbf{r})\\ &+i\kappa\partial_-\psi_\downarrow(\mathbf{r}),\\ \mu\psi_\downarrow(\mathbf{r}) =& -\left(\frac{\partial^2}{\partial x^2}+\frac{\partial^2}{\partial y^2}\right)\psi_\downarrow(\mathbf{r})+V(\mathbf{r})\psi_\downarrow(\mathbf{r})\\ &+g_{\downarrow\downarrow}|\psi_\downarrow(\mathbf{r})|^2\psi_\downarrow(\mathbf{r})+g_{\downarrow\uparrow}|\psi_\uparrow(\mathbf{r})|^2\psi_\downarrow(\mathbf{r})\\ &+i\kappa\partial_+\psi_\uparrow(\mathbf{r}).\end{aligned} \tag{5}$$

Since $V(\mathbf{r})$ and $\psi_{\uparrow,\downarrow}(\mathbf{r})$ are all periodic functions, one can apply Bloch's theorem with the following form:

$$\psi_\sigma(\mathbf{r})=\phi_{\sigma\mathbf{k}}(\mathbf{r})e^{-i\mathbf{k}\cdot\mathbf{r}}, \tag{6}$$

where $\phi_{\sigma\mathbf{k}}$ is a periodic function and $\mathbf{k}$ is the Bloch wave number or the so-called quasimomentum. In particular, from Eq. (5) we obtain the following equation for each Bloch wave state $\phi_{\sigma\mathbf{k}}$:

$$\begin{aligned}\mu(\mathbf{k})\phi_{\uparrow\mathbf{k}}(\mathbf{r}) =& -(\nabla+i\mathbf{k})^2\phi_{\uparrow\mathbf{k}}(\mathbf{r})+V\phi_{\uparrow\mathbf{k}}(\mathbf{r})\\ &+g_{\uparrow\uparrow}|\phi_{\uparrow\mathbf{k}}(\mathbf{r})|^2\phi_{\uparrow\mathbf{k}}(\mathbf{r})+g_{\uparrow\downarrow}|\phi_{\downarrow\mathbf{k}}(\mathbf{r})|^2\phi_{\uparrow\mathbf{k}}(\mathbf{r})\\ &+i\kappa\partial_-\phi_{\downarrow\mathbf{k}}(\mathbf{r}),\\ \mu(\mathbf{k})\phi_{\downarrow\mathbf{k}}(\mathbf{r}) =& -(\nabla+i\mathbf{k})^2\phi_{\downarrow\mathbf{k}}(\mathbf{r})+V\phi_{\downarrow\mathbf{k}}(\mathbf{r})\\ &+g_{\downarrow\downarrow}|\phi_{\downarrow\mathbf{k}}(\mathbf{r})|^2\phi_{\downarrow\mathbf{k}}(\mathbf{r})+g_{\downarrow\uparrow}|\phi_{\uparrow\mathbf{k}}(\mathbf{r})|^2\phi_{\downarrow\mathbf{k}}(\mathbf{r})\\ &+i\kappa\partial_+\phi_{\uparrow\mathbf{k}}(\mathbf{r}).\end{aligned} \tag{7}$$

The set of eigenvalues $\mu(\mathbf{k})$ then forms Bloch bands.

Since gap solitons reside in the linear energy gaps between the Bloch bands [29,30], it is important to first identify the positions of these gaps. To do this, we can discard the nonlinear terms in Eq. (7), by using the Fourier collocation method [68] to numerically diagonalize it and calculate the linear Bloch bands.

The numerical results of the linear Bloch bands of SO-coupled BECs in honeycomb optical lattices are depicted in Fig. 1. Here, we only show the lowest ten Bloch bands as a function of $\mathbf{k}$. In the absence of SOC ($\kappa=0$), the linear eigenequations (7) degenerate into two decoupled equations, and their forms are completely consistent. The linear Bloch bands of the two degenerate eigenequations should be consistent, which is confirmed in Fig. 1(a). We can clearly see the existence of degenerate energy levels and Dirac points. Here, we are very curious about the influence of SOC on the linear Bloch bands. In the presence of SOC (i.e., $\kappa=1$), we show the linear Bloch bands in Fig. 1(b). We can clearly see that

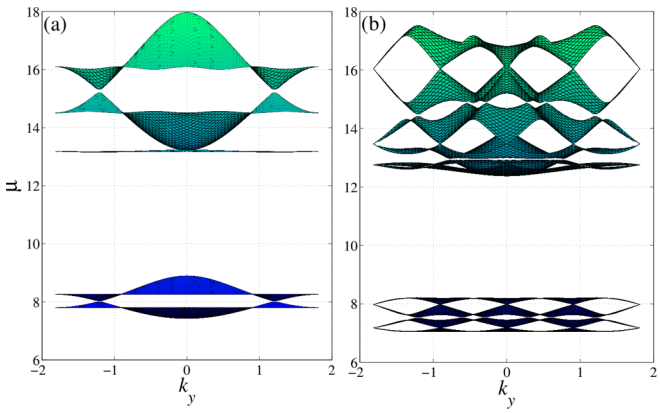

FIG. 1. The linear Bloch band structure of SO-coupled BECs in honeycomb optical lattices. Here, we just showed the axial side view of the Bloch bands. The shaded areas correspond to the linear bands. For comparison, we show (a) the absence of SOC ($\kappa=0$) and (b) the presence of SOC (i.e., $\kappa=1$).

SOC has greatly changed the band structures. First, the degeneracy of the originally completely coincident energy bands is broken, and ten energy bands are prominently displayed. Second, the original Dirac point structures are replaced by a new, richer series of Dirac point structures. These are unique to SOC. At the same time, we can clearly see that the four lowest energy bands have no band gaps due to the degeneracy at the Dirac point. Compared with the absence of SOC, SOC has little effect on the number of band gaps. For the lowest ten energy bands, a significant band gap is formed only between the fourth and fifth energy bands.

Figure 2 shows the effect of lattice depth and SOC on the band gap more clearly. The linear Bloch band gap as a function of depth of the lattice V_0 is shown in Fig. 2(a), where we take SOC strength $\kappa=1$ as an example. For the semi-infinite band gap, its upper boundary increases with the increase of lattice depth V_0. For the first band gap, its upper and lower boundaries increase with the increase of lattice depth V_0. The upper boundary increases faster than the lower

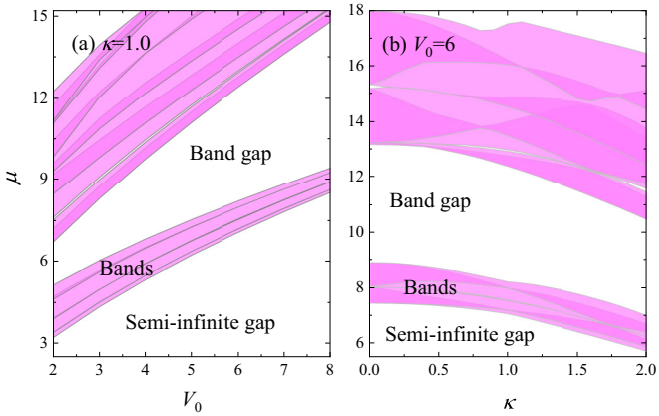

FIG. 2. Linear Bloch spectrum (bands are shaded): (a) as a function of depth of the lattice V_0 with SOC strength $\kappa=1$ and (b) as a function of SOC strength κ with the depth of the lattice $V_0=6$. The shaded areas correspond to the linear bands and the gray lines correspond to the boundaries of the linear bands.

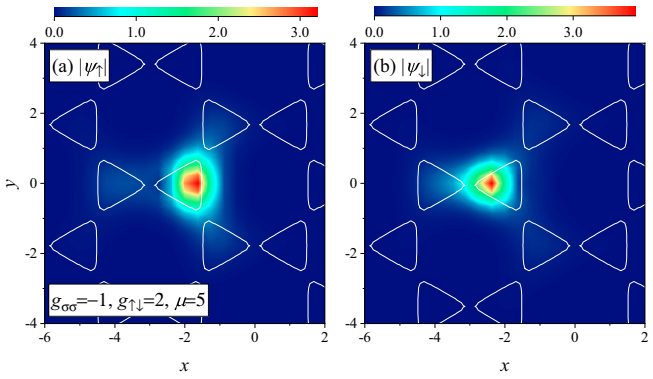

FIG. 3. The vector gap solitons of SO-coupled BECs in honeycomb optical lattices. [(a),(b)] The modulus of the wave functions ($|\psi_\uparrow|$ and $|\psi_\downarrow|$) for spin-up and spin-down states, respectively. Here, we take attractive intraspin atomic interaction $g_{\sigma\sigma} = -1$ and repulsive interspin atomic interaction $g_{\uparrow\downarrow} = 2$ in the semifinite band with $\mu = 5$ as an example. The white solid lines in both panels represent the shape of the schematic honeycomb optical lattice. Compared with the spin-down case, we can see clearly that the spin-up gap solitons have a wider waist and a smaller amplitude. Meanwhile, the two components of the vector gap soliton show phase separations.

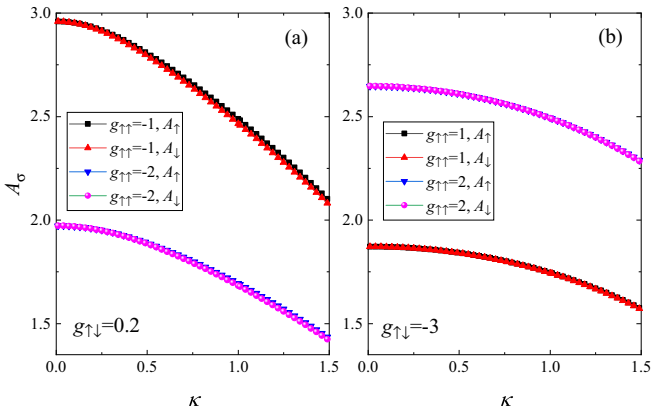

FIG. 4. The amplitudes of vector gap soliton $A_{\sigma=\uparrow,\downarrow}$ vs the SOC strength κ. Here, we focus on the semifinite gap with $\mu = 5$ as an example.

boundary, which causes the width of the first band gap to widen with the increase of lattice depth V_0. Figure 2(b) shows the linear Bloch band gap as a function of SOC κ, where we take $V_0 = 6$ as an example. For the semi-infinite band gap, its upper boundary decreases with the increase of SOC strength κ. For the first band gap, both the upper and lower boundaries decrease with the increase of SOC strength. The width of the first band gap is more sensitive to the lattice depth than the SOC strength.

A gap soliton is a soliton that resides in the linear energy gaps between the Bloch bands. In this paper, we investigate the existence and dynamic stability of gap solitons only in the semifinite gap and first gap.

B. The existence of gap solitons

Gap solitons are spatially localized modes in a gap, which results from the balance between the dispersion and the nonlinearity. For BECs loaded in optical lattices, the dispersion and the nonlinearity originate from the hopping between lattice sites and atomic interaction, respectively. We now proceed to present the numerical results of the vector gap localized modes, which can be constructed through solving Eq. (5) with the initial input being a Gaussian wave packet of the same form for the two spin states. Here, we are looking for gap solitons using the Newton conjugate-gradient method [69], which is one of the powerful numerical techniques to find the solitary wave solutions of a nonlinear evolution equation.

Typical examples of the vector gap solitons, residing within the semifinite band gap, of SO-coupled BECs in honeycomb optical lattices are shown in Fig. 3, where we take attractive intraspin atomic interaction $g_{\sigma\sigma} = -1$ and repulsive interspin atomic interaction $g_{\uparrow\downarrow} = 2$ as an example. It is seen from the figure that both the amplitude and the center position of the density profiles are different for spin-up and spin-down states. We note that in this case, the waist of the two-dimensional gap solitons with spin up is larger than that with spin down, but the amplitude of the gap solitons with spin up is smaller than that with spin down. The two components of the vector gap soliton show phase separation; the center positions of the spin-up and spin-down gap solitons deviate from the center of the lattice site, respectively. The center of the spin-up gap soliton approaches the corner of the triangular lattice, whereas the center of the spin-down gap soliton approaches the foot of the triangular lattice. In fact, the two components of vector gap solitons always show phase separation regardless of whether interspin or intraspin atomic interactions are dominant.

It is interesting to systematically study the effect of the SOC on gap solitons supported by the honeycomb lattice. We find that interestingly, in the regime of weak SOC strength, the configurations of the gap solitons are similar to those in the absence of SOC. In Fig. 4, we show the amplitudes of vector gap soliton $A_{\sigma=\uparrow,\downarrow}$ versus the SOC strength κ. Here, we focus on the semifinite gap with $\mu = 5$ as an example. Figures 4(a) and 4(b) show the dependence of the amplitude of vector gap solitons A with κ for deferent attractive intraspin interaction $g_{\sigma\sigma} = -1$ and -2 with repulsive interspin interaction $g_{\uparrow\downarrow} = 0.2$ and attractive interspin interaction $g_{\uparrow\downarrow} = -3$, respectively. As the SOC strength κ increases, both $A_\uparrow$ and $A_\downarrow$ decrease. Considering that this paper focuses on the regime of weak SOC strength, in the following text, we take $\kappa = 1$ and focus on atomic interactions on the existence and stability of vector gap solitons.

In order to better understand the competition of interspin and intraspin atomic interactions on the existence of vector gap solitons, we show that the amplitude of vector gap solitons varies with the atomic interaction in Fig. 5. Here, we take the semifinite gap with $\mu = 5$ as an example. Figure 5(a) show the dependence of amplitude of vector gap solitons A with interspin interaction $g_{\uparrow\downarrow}$ for different attractive intraspin interactions $g_{\sigma\sigma} = -1$ and -2, from which one can see a sudden transition for the existence of vector gap solitons. Specifically, for attractive interspin interaction $g_{\uparrow\downarrow} < 0$, the amplitudes of the two components of the vector gap soliton are exactly the same, and they both increase with the weakening of the attractive interspin interaction. For the repulsive interspin interaction $g_{\uparrow\downarrow} > 0$, there is an obvious contrast between the

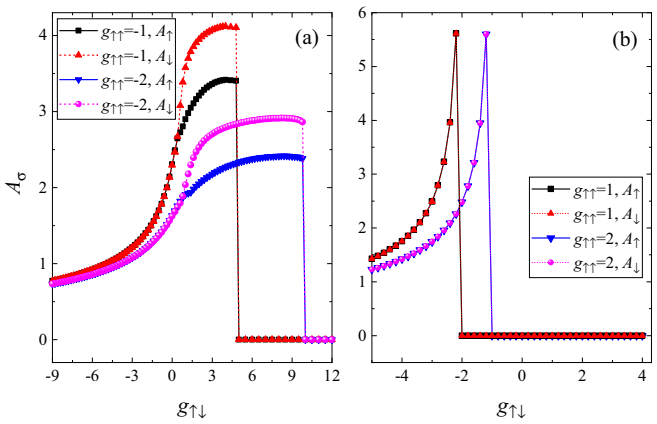

FIG. 5. The existence of vector gap solitons of SO-coupled BECs in honeycomb optical lattices. The amplitudes of the two components of soliton $A_{\sigma=\uparrow,\downarrow}$ vs interspin interaction $g_{\uparrow\downarrow}$ for (a) different attractive intraspin interaction $g_{\sigma\sigma}$ and (b) different repulsive intraspin interaction $g_{\sigma\sigma}$, respectively. Here, we focus on the semifinite gap with $\mu = 5$ as an example.

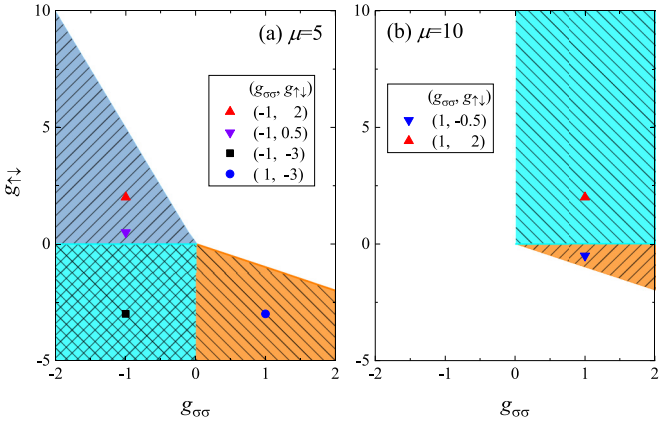

FIG. 6. Phase diagram of the existence of vector gap solitons in the parameter plane ($g_{\sigma\sigma}$, $g_{\uparrow\downarrow}$): (a) for the semifinite band gap with $\mu = 5$ and (b) for the first band gap with $\mu = 10$. The shaded region represents the existence region of vector gap solitons. Shaded regions with different colors represent distinct attractive and repulsive atomic interactions. The marked points with different shapes and colors are representative points in each regime, for which the study of nonlinear dynamics presented below is conducted.

amplitudes of the two components of the vector gap soliton; both of them increase with the enhancement of the repulsive interspin interaction. When the repulsive interspin atomic interaction is large enough, i.e., $g_{\uparrow\downarrow} = 5$ and 10 for $g_{\sigma\sigma} = -1$ and -2, respectively, the amplitude of both components of the vector soliton suddenly becomes zero, and the vector gap solitons are no longer formed. After that, as the repulsive interspin atomic interaction $g_{\uparrow\downarrow}$ continues to increase, the vector solitons are no longer found.

Figure 5(b) shows the dependence of amplitudes of two components of vector gap soliton A with interspin interaction $g_{\uparrow\downarrow}$ for different repulsive intraspin interactions $g_{\sigma\sigma} = 1$ and 2. It is seen from the figure that there is a sudden transition for the existence of vector gap solitons. Specifically, for strong attractive intraspin interaction, vector gap solitons always exist. In the regime of the existence of vector gap solitons, the amplitudes of the two components are always the same. In this case, the amplitudes of the two components of vector gap solitons grow rapidly with the weakening of the attractive interspin interaction $g_{\uparrow\downarrow}$. When the attractive interspin interaction weakens to a critical value, i.e., $g_{\uparrow\downarrow} = -1$ and -2 for $g_{\sigma\sigma} = 1$ and 2, respectively, its amplitude reaches the maximum. After that, as the attractive interspin atomic interaction $g_{\uparrow\downarrow}$ continues to decrease, the amplitude of the vector soliton suddenly becomes zero, and the solitons are no longer formed. At the same time, we noticed that when the interspin atomic interaction $g_{\uparrow\downarrow}$ changes from attractive to repulsive, the vector gap solitons no longer exist regardless of the strength of the repulsive interspin atomic interaction.

For now, we focus on the semifinite gap and first band gap, within which the vector gap solitons may be localized due to the interplay between the interspin and intraspin atomic interaction. With an in-depth investigation, we numerically seek the relationships between intraspin atomic interaction $g_{\sigma\sigma}$ and interspin atomic interaction $g_{\uparrow\downarrow}$ on the existence of vector gap solitons.

The existence of vector gap solitons in the semifinite band gap with $\mu = 5$ is shown in Fig. 6(a), which shows the obvious boundary for the existence of solitons in the parameter plane of intraspin atomic interaction and interspin atomic interaction ($g_{\sigma\sigma}$, $g_{\uparrow\downarrow}$).

(i) For the regime in which both the intraspin and interspin atomic interaction are attractive, i.e., $g_{\sigma\sigma} < 0$, and $g_{\uparrow\downarrow} < 0$, vector gap solitons always exist.

(ii) For the regime in which both the intraspin and interspin atomic interaction are repulsive, i.e., $g_{\sigma\sigma} > 0$, and $g_{\uparrow\downarrow} > 0$, vector gap solitons do not exist.

(iii) For the regime in which the intraspin atomic interaction is attractive, while the interspin atomic interaction is repulsive, i.e., $g_{\sigma\sigma} < 0$, and $g_{\uparrow\downarrow} > 0$, vector gap solitons only exist when the attractive intraspin atomic interaction is weaker than one-fifth of the repulsive interaction interspin atomic interaction, i.e., $|g_{\sigma\sigma}| > |g_{\uparrow\downarrow}|/5$.

(iv) For the regime in which the intraspin atomic interaction is repulsive, while the interspin atomic interaction is attractive, i.e., $g_{\sigma\sigma} > 0$ and $g_{\uparrow\downarrow} < 0$, vector gap solitons only exist when the attractive interspin atomic interaction $g_{\uparrow\downarrow}$ is stronger than the repulsive interaction intraspin atomic interaction $g_{\sigma\sigma}$, i.e., $|g_{\sigma\sigma}| < |g_{\uparrow\downarrow}|$. It can be seen that for the semi-infinite gap to form a gap soliton, at least one of the intraspin and interspin atomic interactions should be attractive, and the attractive interaction should be stronger than the repulsive interaction.

Figure 6(b) shows the existence of vector gap solitons in the first band gap with $\mu = 10$. Also shown is the obvious boundary for the existence of solitons in the parameter space of intraspin and interspin atomic interaction ($g_{\sigma\sigma}$, $g_{\uparrow\downarrow}$). Compared with the case of the semi-infinite gap, the region where vector solitons exist in the first band gap is smaller, and it is almost the opposite region of the semi-infinite one. Specifically, we have the following.

(i) For the regime in which the intraspin atomic interaction is attractive, i.e., $g_{\sigma\sigma} < 0$, vector gap solitons always do not exist regardless of whether the interspin atomic interaction

$g_{\uparrow\downarrow}$ is repulsive or attractive. Vector gap solitons always do not exist.

(ii) For the regime in which both the intraspin and interspin atomic interaction are repulsive, i.e., $g_{\sigma\sigma} > 0$, and $g_{\uparrow\downarrow} > 0$, vector gap solitons always exist.

(iii) For the regime in which the intraspin atomic interaction is repulsive, while the interspin atomic interaction is attractive, i.e., $g_{\sigma\sigma} > 0$ and $g_{\uparrow\downarrow} < 0$, vector gap solitons only exist when the repulsive intraspin atomic interaction $g_{\sigma\sigma}$ is stronger than the attractive interspin atomic interaction $g_{\uparrow\downarrow}$, i.e., $|g_{\sigma\sigma}| > |g_{\uparrow\downarrow}|$. It can be seen that for the first band gap to form gap solitons, either both the intraspin and the interspin atomic interaction are repulsive, or the repulsive intraspin atomic interaction is stronger than the attractive interspin atomic interaction.

We can clearly see that the existence of vector gap solitons of SO-coupled BECs in honeycomb optical lattices is highly dependent on the properties of atomic interaction.

IV. NONLINEAR DYNAMICAL STABILITIES OF VECTOR GAP SOLITONS

Stability of extended and localized modes in nonlinear systems is a very important issue, since only dynamically stable modes are likely to be generated and observed in experiments. In this section, we examine the stability of the vector gap modes by using the direct evolution dynamics, and discuss their physical intension. To trigger potential dynamic instabilities, a 1% Gaussian distributed noise is added to the initial gap solitons. Then, we numerically propagate Eq. (3) by the time-splitting Fourier spectral method. We respectively discuss the nonlinear dynamic evolution of solitons in the semi-infinite band gap and the first band gap in detail.

A. In the semifinite gap

For the semi-infinite band gap, in the parameter space ($g_{\sigma\sigma}$, $g_{\uparrow\downarrow}$), the gap soliton exists in three parameter regions according to the atomic interaction properties: (i) in the second quadrant with $|g_{\uparrow\downarrow}| < 5|g_{\sigma\sigma}|$, (ii) in the third quadrant, and (iii) in the fourth quadrant with $|g_{\uparrow\downarrow}| < |g_{\sigma\sigma}|$. We discuss the stability of vector gap solitons in these three regions respectively.

1. Case (i): In the second quadrant with $|g_{\uparrow\downarrow}| < 5|g_{\sigma\sigma}|$

In this parameter region, the intraspin atomic interaction is attractive, while the interspin atomic interaction is repulsive, i.e., $g_{\sigma\sigma} < 0$ and $g_{\uparrow\downarrow} > 0$. As might be expected, the stability of the vector gap solitons is different for $|g_{\uparrow\downarrow}| < |g_{\sigma\sigma}|$ and $|g_{\sigma\sigma}| < |g_{\uparrow\downarrow}| < 5|g_{\sigma\sigma}|$.

In Fig. 7, we show the time evolution of vector gap solitons in the semi-infinite gap in the second quadrant with $|g_{\sigma\sigma}| < |g_{\uparrow\downarrow}| < 5|g_{\sigma\sigma}|$. Here, we take $g_{\sigma\sigma} = -1$, $g_{\uparrow\downarrow} = 2$ [corresponding to the red upper triangle in Fig. 6(a)] as an example. We can see that the spin-up and spin-down profiles of the vector gap soliton are initially located in the same lattice. The centers of spin-up and spin-down profiles deviate from the center of the lattice in the opposite direction. In fact, the stronger the interspin repulsive atomic interaction, the farther the deviation (of course, when the interspin repulsive atomic interaction exceeds five times the intraspin attractive atomic interaction, the vector gap solitons will not exist). To trigger potential dynamic instabilities, a 1% Gaussian distributed noise was added to the initial gap solitons. It can be seen that the amplitude and waist of the two components of the vector gap soliton are all changed. Specifically, the amplitude of the spin-up profile of the vector gap soliton increases with time, while the amplitude of the spin-down profile of the vector gap soliton decreases with time. Meanwhile, the waist of the spin-up profile becomes thinner with the evolution of time. Clearly, in such a case, vector gap solitons are dynamically unstable. In fact, this represents spin polarization due to SOC.

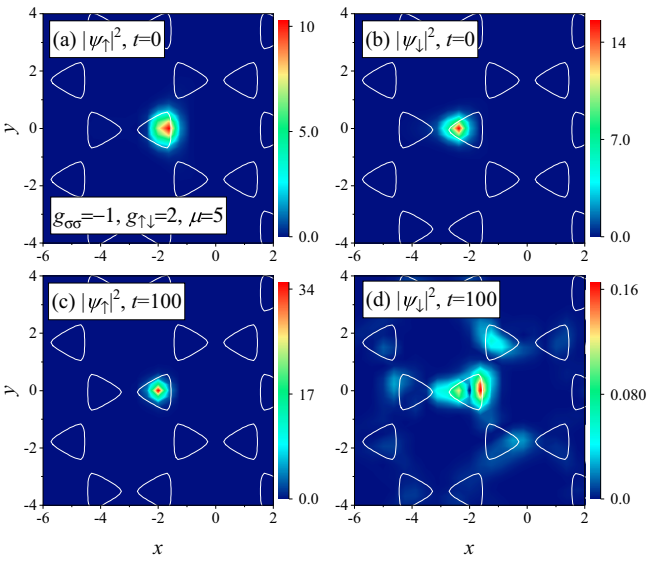

FIG. 7. Time evolution of vector gap solitons in the semi-infinite gap with $\mu = 5$. Here, we focus on the second quadrant with $5|g_{\sigma\sigma}| > |g_{\uparrow\downarrow}| > |g_{\sigma\sigma}|$. We take $g_{\sigma\sigma} = -1$, $g_{\uparrow\downarrow} = 2$ [corresponding to the red upper triangle in Fig. 6(a)] as an example. A small perturbation of 1% Gaussian distributed noise was added to the initial gap solitons to trigger potential instabilities. (a, b) The initial density profiles for spin-up and spin-down states, respectively. [(c),(d)] The final ($t = 100$) density profiles for spin-up and spin-down states, respectively. In this case, the spin-down state of the vector gap soliton collapses and the spin-up state of the vector gap soliton is trapped and raised. This represents spin polarization due to SOC.

The time evolution of vector gap solitons in the semi-infinite gap in the second quadrant with $|g_{\uparrow\downarrow}| < |g_{\sigma\sigma}|$ is shown in Fig. 8. Here, we take $g_{\sigma\sigma} = -1$, $g_{\uparrow\downarrow} = 0.5$ [corresponding to the purple lower triangle in Fig. 6(a)] as an example. We compare gap solitons in Fig. 8 with those in Fig. 7; although the centers of the two components of the vector gap soliton still deviate in the opposite direction, the distance of deviation becomes smaller, which results from the decrease of the repulsive atomic interactions. In particular, with time evolution, distribution of the vector gap solitons is exactly the same as that of the initial states. Clearly, in such a case, vector gap solitons are dynamically stable.

From the above comprehensive analysis, we could draw a conclusion that vector gap solitons in the semi-infinite gap in the second quadrant with $|g_{\uparrow\downarrow}| < |g_{\sigma\sigma}|$ are dynamically stable, whereas with $|g_{\sigma\sigma}| < |g_{\uparrow\downarrow}| < 5|g_{\sigma\sigma}|$ they are unstable.

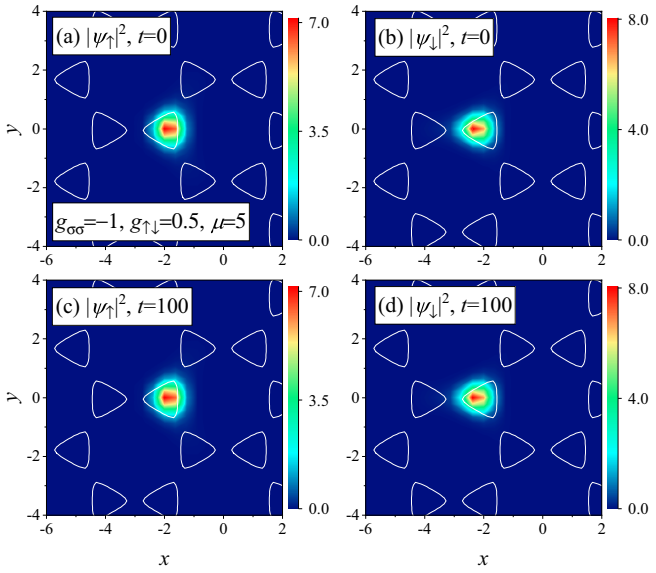

FIG. 8. Time evolution of vector gap solitons in the semi-infinite gap with $\mu = 5$. Here, we focus on the second quadrant with $|g_{\sigma\sigma}| > |g_{\uparrow\downarrow}|$. We take $g_{\sigma\sigma} = -1$, $g_{\uparrow\downarrow} = 0.5$ [corresponding to the purple lower triangle in Fig. 6(a)] as an example. A 1% Gaussian distributed noise was added to the initial gap solitons to trigger potential instabilities. [(a),(b)] The initial density profiles for spin-up and spin-down states, respectively. [(c),(d)] The final ($t = 100$) density profiles for spin-up and spin-down states, respectively. In this case, both states of the vector gap soliton are stably trapped in the initial lattice.

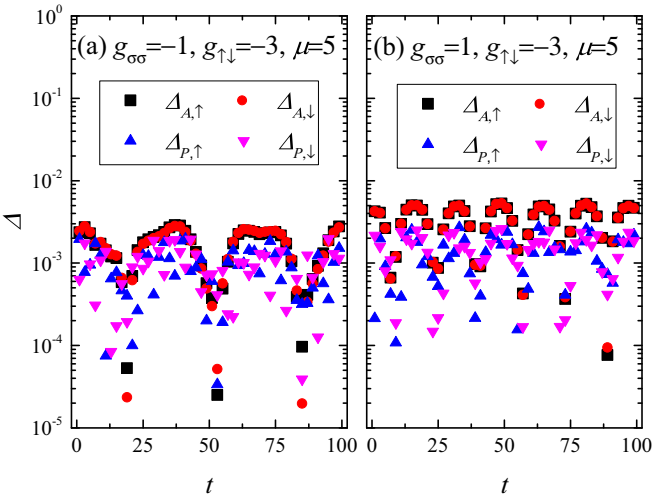

FIG. 9. The time dependence of ratio $\Delta_{A,\sigma}$ and $\Delta_{P,\sigma}$ in the semi-infinite gap with $\mu = 5$. (a) In the third quadrant with $g_{\sigma\sigma} < 0$ and $g_{\uparrow\downarrow} < 0$. Here, we take $g_{\sigma\sigma} = -1$, $g_{\uparrow\downarrow} = -3$ [corresponding to the black square in Fig. 6(a)] as an example. (b) In the fourth quadrant with $|g_{\sigma\sigma}| < |g_{\uparrow\downarrow}|$. We take $g_{\sigma\sigma} = 1$, $g_{\uparrow\downarrow} = -3$ [corresponding to the blue circle in Fig. 6(a)] as an example. For both cases, a 1% Gaussian distributed noise was added to the initial gap solitons to trigger potential instabilities.

2. *Case (ii): In the third quadrant*

In this parameter region, both the intra- and interspin atomic interaction are attractive, i.e., $g_{\sigma\sigma} < 0$ and $g_{\uparrow\downarrow} < 0$. In order to study the nonlinear dynamical stabilities of vector gap solitons more clearly, we pay attention to time dependence of the amplitude and the total power of gap solitons. In order to see this, we define the amplitude A and the total power P of the gap solitons as

$$A_\sigma(t) = \max\left[|\psi_\sigma(t)|\right], \quad P_\sigma(t) = \int |\psi_\sigma(t)|^2 dxdy. \tag{8}$$

In order to characterize the stability of solitons, we introduce the following two sets of ratios:

$$\Delta_{A,\sigma}(t) = \frac{|A_\sigma(t) - A_\sigma(0)|}{A_\sigma(0)},$$
$$\Delta_{P,\sigma}(t) = \frac{|P_\sigma(t) - P_\sigma(0)|}{P_\sigma(0)}. \tag{9}$$

These two sets of quantities, respectively, represent the changes of amplitude and power of solitons in the process of dynamic evolution. Obviously, the closer they are to zero, the more similar they are to the initial state, and the more stable the soliton is. In contrast, the larger they are, the farther the soliton is from the initial state.

The time dependences of ratios $\Delta_{A,\sigma}$ and $\Delta_{P,\sigma}$ in the semi-infinite gap with $\mu = 5$ for the third quadrant of the parameter plane ($g_{\sigma\sigma}$, $g_{\uparrow\downarrow}$) are shown in Fig. 9. Here, we take $g_{\sigma\sigma} = 1$, $g_{\uparrow\downarrow} = -3$ [corresponding to the black square in Fig. 6(a)] as an example. To trigger potential dynamic instabilities, we add a 1% Gaussian distributed noise to the initial gap solitons. It can be seen that the ratios of all these quantities for both the spin-up and spin-down gap solitons do not exceed the amount of initial disturbance. Clearly, in such a case, vector gap solitons are dynamically stable. In fact, we randomly selected many vector gap solitons in this region and observed their dynamic processes. We find that all of the gap solitons in this region are dynamically stable.

3. *Case (iii): In the fourth quadrant with $|g_{\sigma\sigma}| < |g_{\uparrow\downarrow}|$*

The existence of vector gap solitons in this region should satisfy that the intraspin attractive atomic interaction is stronger than the interspin repulsive atomic interaction, i.e., $|g_{\sigma\sigma}| < |g_{\uparrow\downarrow}|$. Therefore, in this region, there is still competition between repulsive and attractive atomic interactions. The amplitude, waist, and center of the two components of the vector solitons are almost the same due to the stronger attractive atomic interactions. We also use the time dependence of ratio $\Delta_{A,\sigma}$ and $\Delta_{P,\sigma}$ to check the stability of vector gap solitons in this regime. The results are shown in Fig. 9(b). Here, we take $g_{\sigma\sigma} = 1$, $g_{\uparrow\downarrow} = -3$ [corresponding to the blue circle in Fig. 6(a)] as an example. To trigger potential dynamic instabilities, we add a 1% Gaussian distributed noise to the initial state. We can clearly see that in the process of evolution, for both the spin-up and spin-down gap solitons, these ratios do not exceed the amount of initial disturbance. Actually, in this region, we numerically tested the dynamic evolution of a large number of vector gap solitons, and the results showed that they are all stable.

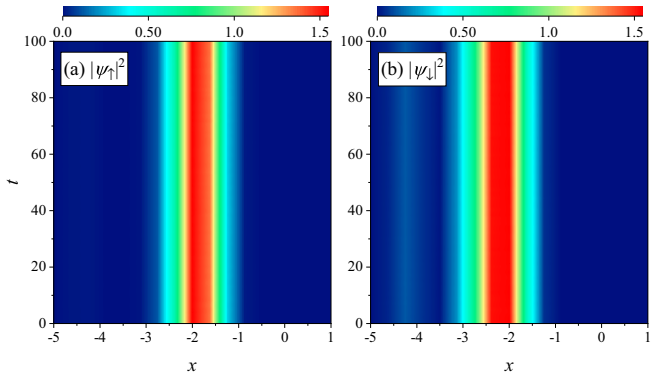

FIG. 10. Time evolution of vector gap solitons in the first gap with $\mu = 10$. Here, we show the evolution of the cross section at $y = 0$ with time in detail. Here, we focus on the first quadrant in parameter space ($g_{\sigma\sigma}$, $g_{\uparrow\downarrow}$), and take $g_{\sigma\sigma} = 1$, $g_{\uparrow\downarrow} = 2$ [corresponding to the red upper triangle in Fig. 6(b)] as an example. A 1% Gaussian distributed noise was added to the initial gap solitons to trigger potential instabilities. (a, b) The evolution of the cross section of density profiles for spin-up and spin-down states, respectively. In this case, both components of the vector gap soliton remain trapped in the initial state.

B. In the first gap

For the first band gap, in the parameter space ($g_{\sigma\sigma}$, $g_{\uparrow\downarrow}$), the gap soliton exists in two parameter regions according to the atomic interaction properties: (i) in the first quadrant and (ii) in the fourth quadrant with $|g_{\sigma\sigma}| < |g_{\uparrow\downarrow}|$. In the following, we check the stability of vector gap solitons in these two regions, respectively.

1. Case (i): In the first quadrant

In this region, both the intraspin and the interspin atomic interaction are repulsive, and the vector gap solitons always exist in the first gap. The nonlinear dynamics for the vector gap solitons with $g_{\sigma\sigma} = 1$, $g_{\uparrow\downarrow} = 2$ [corresponding to the red upper triangle in Fig. 6(b)] are shown in Fig. 10, where a 1% Gaussian distributed noise was added to the initial gap solitons to trigger potential instabilities. Here, we show the evolution of the cross section at $y = 0$ with time in detail. Figures 10(a) and 10(b) denote the evolution of the cross section at $y = 0$ for spin-up and spin-down states, respectively. One can clearly see that the amplitude, waist, and center of the two components of the vector solitons are almost the same during evolution. In Fig. 11(a), we also show the time dependence of ratios $\Delta_{A,\sigma}$ and $\Delta_{P,\sigma}$ for vector gap solitons. We can clearly see that these ratios never exceed the amount of the initial disturbance. In this parameter region, we also randomly selected a large number of vector gap solitons to demonstrate their dynamics and found that they are all stable.

2. Case (ii): In the fourth quadrant with $|g_{\uparrow\downarrow}| < |g_{\sigma\sigma}|$

Now, we focus on dynamic stability of vector gap solitons in the fourth quadrant. The existence of vector gap solitons in the fourth quadrant should satisfy that the repulsive intraspin atomic interaction is stronger than the attractive interspin atomic interaction, i.e., $|g_{\uparrow\downarrow}| < |g_{\sigma\sigma}|$. The time dependences

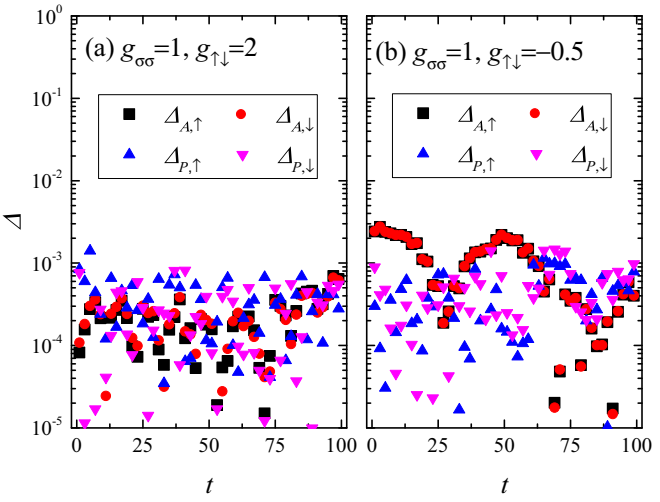

FIG. 11. The time dependence of ratio $\Delta_{A,\sigma}$ and $\Delta_{P,\sigma}$ for vector gap solitons in the first gap with $\mu = 10$. (a) In the first quadrant, we take $g_{\sigma\sigma} = 1$, $g_{\uparrow\downarrow} = 2$ [corresponding to the red upper triangle in Fig. 6(b)] as an example. (b) In the fourth quadrant with $|g_{\uparrow\downarrow}| < |g_{\sigma\sigma}|$. We take $g_{\sigma\sigma} = 1$, $g_{\uparrow\downarrow} = -0.5$ [corresponding to the blue lower triangle in Fig. 6(b)] as an example. For both cases, a 1% Gaussian distributed noise was added to the initial gap solitons to trigger potential instabilities.

of ratios $\Delta_{A,\sigma}$ and $\Delta_{P,\sigma}$ for vector gap solitons with $g_{\sigma\sigma} = 1$, $g_{\uparrow\downarrow} = -0.5$ [corresponding to the blue lower triangle in Fig. 6(b)] are shown in Fig. 11(b). To trigger potential instabilities, we add a 1% Gaussian distributed noise to the initial gap solitons. One can clearly see that the amplitude and power of the two components of the vector solitons are almost the same. With the evolution of time, the ratios of all these quantities for both the spin-up and spin-down gap solitons do not exceed the amount of initial disturbance. Clearly, in such a case, vector gap solitons are dynamically stable.

V. CONCLUSIONS

To summarize, we have investigated the formation and dynamic instabilities of vector gap solitons of SO-coupled BECs in honeycomb optical lattices. We focus on both the interspin and intraspin atomic interactions on the existences and nonlinear dynamics stability. It is worth emphasizing that the two spin states of the vector gap soliton always show phase separation regardless of whether interspin or intraspin atomic interactions are dominant. The main results for both the semi-infinite gap and first gap are summarized in Fig. 12.

In this paper, we investigate the existence and dynamic stability of gap solitons only in the semifinite gap and first gap. The existence of vector gap solitons of SO-coupled BECs in honeycomb optical lattices is highly dependent on the properties of atomic interaction. For the semi-infinite gap, as shown in the left panel in Fig. 12, to form gap solitons, at least one of the intraspin and interspin atomic interactions should be attractive, and the attractive interaction should be stronger than the repulsive interaction. For the first gap, as shown in the right panel in Fig. 12, to form gap solitons,

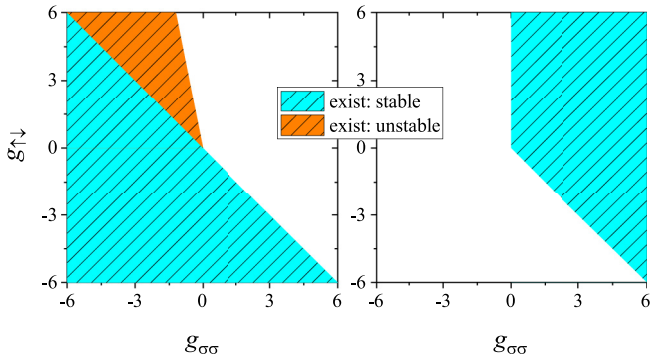

FIG. 12. Summary of the existences and nonlinear dynamics stability of vector gap solitons in the parameter plane ($g_{\sigma\sigma}$, $g_{\uparrow\downarrow}$). The left and right show the semi-infinite band gap and first band gap, respectively. The shaded region represents the existence region of vector gap solitons. Shaded regions with different colors represent distinct regions for stable and unstable gap solitons.

either both the intraspin and the interspin atomic interaction are repulsive, or the repulsive intraspin atomic interaction is stronger than the attractive interspin atomic interaction. We examine the stability of these vector gap modes by using the direct evolution dynamics. We randomly select a large number of vector gap solitons to demonstrate their dynamics and find that the vector gaps in the first gap are all stable, whereas there are stable and unstable regions in the parameter space ($g_{\sigma\sigma}$, $g_{\uparrow\downarrow}$), as shown in different colors in Fig. 12.

Based on our simulations, we propose a scheme for experimental observation of the gap solitons. In real experiments, one can consider a mixture of BECs composed of the two internal states of ^{87}Rb [63], namely, $|\uparrow\rangle \equiv |F = 1, m_F = 0\rangle$ and $|\downarrow\rangle \equiv |F = 1, m_F = -1\rangle$. In real experiments, the system contains about 1.8×10^5 atoms. The BECs with Rashba SOC are loaded in a honeycomb optical lattice, which is generated experimentally by superposing three coplanar traveling laser beams [65,66]. The strength of SOC can be precisely controlled by optics means. The the intra- and interspin interactions can be changed by modifying atomic collisions, which are experimentally feasible due to the flexible and precise control of the scattering lengths achievable by magnetically tuning the Feshbach resonances [70]. Our paper extends the studies of BECs in optical lattices. We hope that these types of spatially localized condensate can potentially be observed in further experiments.

ACKNOWLEDGMENTS

This work is supported by the National Natural Science Foundation of China (Grants No. 12065022, No. 12005173, and No. 12365004), the Natural Science Foundation of Gansu Province (Grant No. 20JR10RA082), and the China Postdoctoral Science Foundation (Grant No. 2020M680318).

[1] M. Z. Hasan and C. L. Kane, Rev. Mod. Phys. **82**, 3045 (2010).
[2] X.-L. Qi and S.-C. Zhang, Rev. Mod. Phys. **83**, 1057 (2011).
[3] M. Z. Hasan, G. Chang, I. Belopolski, G. Bian, S.-Y. Xu, and J.-X. Yin, Nat. Rev. Mater. **6**, 784 (2021).
[4] M. Sato and Y. Ando, Rep. Prog. Phys. **80**, 076501 (2017).
[5] X.-L. Qi, Y.-S. Wu, and S.-C. Zhang, Phys. Rev. B **74**, 085308 (2006).
[6] P. Wölfle, Rep. Prog. Phys. **81**, 032501 (2018).
[7] S.-L. Zhu, H. Fu, C.-J. Wu, S.-C. Zhang, and L.-M. Duan, Phys. Rev. Lett. **97**, 240401 (2006).
[8] N. H. Lindner, G. Refael, and V. Galitski, Nat. Phys. **7**, 490 (2011).
[9] M. S. Rudner, N. H. Lindner, E. Berg, and M. Levin, Phys. Rev. X **3**, 031005 (2013).
[10] P. Wang, Z.-Q. Yu, Z. Fu, J. Miao, L. Huang, S. Chai, H. Zhai, and J. Zhang, Phys. Rev. Lett. **109**, 095301 (2012).
[11] L. W. Cheuk, A. T. Sommer, Z. Hadzibabic, T. Yefsah, W. S. Bakr, and M. W. Zwierlein, Phys. Rev. Lett. **109**, 095302 (2012).
[12] Y.-J. Lin, R. L. Compton, A. R. Perry, W. D. Phillips, J. V. Porto, and I. B. Spielman, Phys. Rev. Lett. **102**, 130401 (2009).
[13] Y.-J. Lin, R. L. Compton, K. Jimenez-Garcia, J. V. Porto, and I. B. Spielman, Nature (London) **462**, 628 (2009).
[14] T. Kawakami, T. Mizushima, M. Nitta, and K. Machida, Phys. Rev. Lett. **109**, 015301 (2012).
[15] H. Flayac, D. D. Solnyshkov, I. A. Shelykh, and G. Malpuech, Phys. Rev. Lett. **110**, 016404 (2013).
[16] C.-F. Liu, G. Juzeliūnas, and W. M. Liu, Phys. Rev. A **95**, 023624 (2017).
[17] V. Achilleos, D. J. Frantzeskakis, P. G. Kevrekidis, and D. E. Pelinovsky, Phys. Rev. Lett. **110**, 264101 (2013).
[18] Y. Xu, Y. Zhang, and B. Wu, Phys. Rev. A **87**, 013614 (2013).
[19] L. Wen, Q. Sun, Y. Chen, D.-S. Wang, J. Hu, H. Chen, W.-M. Liu, G. Juzeliūnas, B. A. Malomed, and A.-C. Ji, Phys. Rev. A **94**, 061602(R) (2016).
[20] S. K. Adhikari, Phys. Rev. A **100**, 063618 (2019).
[21] W. B. Cardoso and R. M. P. Teixeira, Nonlinear Dyn. **96**, 1147 (2019).
[22] Y. V. Kartashov and D. A. Zezyulin, Phys. Rev. Lett. **122**, 123201 (2019).
[23] Y. V. Kartashov and V. V. Konotop, Phys. Rev. Lett. **125**, 054101 (2020).
[24] Y.-J. Wang, L. Wen, G.-P. Chen, S.-G. Zhang, and X.-F. Zhang, New J. Phys. **22**, 033006 (2020).
[25] X.-w. Chen, Z.-g. Deng, X.-x. Xu, S.-l. Li, Z.-w. Fan, Z.-p. Chen, B. Liu, and Y.-y. Li, Nonlinear Dyn. **101**, 569 (2020).
[26] D. B. Belobo and T. Meier, New J. Phys. **23**, 043045 (2021).
[27] S. K. Adhikari, Phys. Rev. E **104**, 024207 (2021).
[28] O. Morsch and M. Oberthaler, Rev. Mod. Phys. **78**, 179 (2006).
[29] F. Lederer, G. I. Stegeman, D. N. Christodoulides, G. Assanto, M. Segev, and Y. Silberberg, Phys. Rep. **463**, 1 (2008).
[30] Y. V. Kartashov, B. A. Malomed, and L. Torner, Rev. Mod. Phys. **83**, 247 (2011).
[31] A. Aceves and S. Wabnitz, Phys. Lett. A **141**, 37 (1989).
[32] D. N. Christodoulides and R. I. Joseph, Phys. Rev. Lett. **62**, 1746 (1989).
[33] C. M. de Sterke and J. E. Sipe, in *Progress in Optics*, edited by E. Wolf (Elsevier, Amsterdam, 1994), Vol. 33, pp. 203–260.

[34] D. E. Pelinovsky, A. A. Sukhorukov, and Y. S. Kivshar, Phys. Rev. E **70**, 036618 (2004).
[35] J. Su, H. Lyu, Y. Chen, and Y. Zhang, Phys. Rev. A **104**, 043315 (2021).
[36] B. J. Eggleton, R. E. Slusher, C. M. de Sterke, P. A. Krug, and J. E. Sipe, Phys. Rev. Lett. **76**, 1627 (1996).
[37] P. Meystre, *Atom Optics* (Springer-Verlag, Berlin, 2001).
[38] V. A. Brazhnyi and V. V. Konotop, Mod. Phys. Lett. B **18**, 627 (2004).
[39] R. Carretero-González, D. J. Frantzeskakis, and P. G. Kevrekidis, Nonlinearity **21**, R139 (2008).
[40] E. A. Ostrovskaya and Y. S. Kivshar, Phys. Rev. Lett. **90**, 160407 (2003).
[41] B. Eiermann, T. Anker, M. Albiez, M. Taglieber, P. Treutlein, K.-P. Marzlin, and M. K. Oberthaler, Phys. Rev. Lett. **92**, 230401 (2004).
[42] Y. V. Kartashov, V. V. Konotop, and F. K. Abdullaev, Phys. Rev. Lett. **111**, 060402 (2013).
[43] M. Salerno, F. K. Abdullaev, A. Gammal, and L. Tomio, Phys. Rev. A **94**, 043602 (2016).
[44] V. E. Lobanov, Y. V. Kartashov, and V. V. Konotop, Phys. Rev. Lett. **112**, 180403 (2014).
[45] Y. Zhang, Y. Xu, and T. Busch, Phys. Rev. A **91**, 043629 (2015).
[46] X. Zhu, H. Li, and Z. Shi, Phys. Lett. A **380**, 3253 (2016).
[47] F. K. Abdullaev, M. Brtka, A. Gammal, and L. Tomio, Phys. Rev. A **97**, 053611 (2018).
[48] Y. Li, Y. Liu, Z. Fan, W. Pang, S. Fu, and B. A. Malomed, Phys. Rev. A **95**, 063613 (2017).
[49] H. Sakaguchi and B. A. Malomed, Phys. Rev. A **97**, 013607 (2018).
[50] Z. Fan, Z. Chen, Y. Li, and B. A. Malomed, Phys. Rev. A **101**, 013607 (2020).
[51] Y. V. Kartashov, E. Y. Sherman, B. A. Malomed, and V. V. Konotop, New J. Phys. **22**, 103014 (2020).
[52] S. Smirnov, D. Bercioux, and M. Grifoni, Europhys. Lett. **80**, 27003 (2007).
[53] V. Y. Demikhovskiĭ, D. V. Khomitsky, and A. A. Perov, J. Low Temp. Phys. **33**, 115 (2007).
[54] C. Becker, P. Soltan-Panahi, J. Kronjäger, S. Dörscher, K. Bongs, and K. Sengstock, New J. Phys. **12**, 065025 (2010).
[55] L. Tarruell, D. Greif, T. Uehlinger, G. Jotzu, and T. Esslinger, Nature (London) **483**, 302 (2012).
[56] G.-B. Jo, J. Guzman, C. K. Thomas, P. Hosur, A. Vishwanath, and D. M. Stamper-Kurn, Phys. Rev. Lett. **108**, 045305 (2012).
[57] M. J. Ablowitz and Y. Zhu, Nonlinear dynamics of Bloch wave packets in honeycomb lattices, in *Spontaneous Symmetry Breaking, Self-Trapping, and Josephson Oscillations*, edited by B. A. Malomed (Springer-Verlag, Berlin, 2013), pp. 1–26.
[58] O. Peleg, G. Bartal, B. Freedman, O. Manela, M. Segev, and D. N. Christodoulides, Phys. Rev. Lett. **98**, 103901 (2007).
[59] K. J. H. Law, H. Susanto, and P. G. Kevrekidis, Phys. Rev. A **78**, 033802 (2008).
[60] P. G. Kevrekidis, B. A. Malomed, and Y. B. Gaididei, Phys. Rev. E **66**, 016609 (2002).
[61] H. Meng, Y. Zhou, X. Li, X. Ren, X. Wan, Z. Zhou, W. Wang, and Y. Shi, Physica A **577**, 126087 (2021).
[62] H. Meng, Y. Zhou, X. Ren, X. Wan, J. Zhang, J. Wang, X. Fan, W. Wang, and Y. Shi, Chin. Phys. B **30**, 126701 (2021).
[63] Y.-J. Lin, K. Jiménez-García, and I. B. Spielman, Nature (London) **471**, 83 (2011).
[64] M. Egorov, B. Opanchuk, P. Drummond, B. V. Hall, P. Hannaford, and A. I. Sidorov, Phys. Rev. A **87**, 053614 (2013).
[65] G. Grynberg, B. Lounis, P. Verkerk, J.-Y. Courtois, and C. Salomon, Phys. Rev. Lett. **70**, 2249 (1993).
[66] B. Wunsch, F. Guinea, and F. Sols, New J. Phys. **10**, 103027 (2008).
[67] M. J. Ablowitz and Y. Zhu, Phys. Rev. A **82**, 013840 (2010).
[68] J. Yang, *Nonlinear Waves in Integrable and Nonintegrable Systems* (SIAM, Philadelphia, 2010).
[69] J. Yang, J. Comput. Phys. **228**, 7007 (2009).
[70] C. Chin, R. Grimm, P. Julienne, and E. Tiesinga, Rev. Mod. Phys. **82**, 1225 (2010).